AIAA JOURNAL
Vol. 33, No. 1, January 1995

Closed-Form Expressions for Higher Order Electroelastic Tetrahedral Elements

Mohammad A. Moetakef,* Kent L. Lawrence,† Shiv P. Joshi,‡ and Panayiotis S. Shiakolas§
University of Texas at Arlington, Arlington, Texas 76019

A finite element formulation for three-dimensional modeling of dynamic and static responses of structures with piezoelectric components and the development of highly efficient closed-form expressions for element electroelastic stiffness matrices for straight-sided linear strain tetrahedral and quadratic strain tetrahedral elements are presented. Included is a discussion of procedures for combining tetrahedra to produce hexahedral elements. Two simple numerical examples are presented to illustrate the formulation.

Introduction

THE finite element formulation for piezoelectric continua was first presented by Allik and Hughes over 20 years ago.[1] In their pioneering work they established the principles involved in the formulation of electroelastic finite elements with the implementation of a constant strain tetrahedral (CST) element. Over the last decade increasing interest in utilizing the piezoelectric effect in the design of smart materials and structures has motivated other researchers to develop new solid elements with incorporated piezoelectric effect.[2,3]

Although the division of an arbitrary volume into individual brick elements does not involve visualization difficulties or a high chance of nodal numbering error, it is often necessary to use tetrahedra to complete the subdivisions at curved boundaries. With advances in computer graphics and automatic mesh generation routines, the automatic development of tetrahedral element meshes has become commonplace.

Considerable advancement has also been achieved in the use of computers to perform symbolic mathematical operations. The application of symbolic computation in the finite element analysis dates back to the late 1970s.[4] A primary application of this approach is focused on the generation of explicit forms for element stiffness matrices and equivalent nodal load vectors.[5,6] Shiakolas et al.[6] presented closed-form element stiffness matrices and equivalent nodal loads for linear strain tetrahedral (LST) and quadratic strain tetrahedral (QST) elements with straight sides. It was found that the element formulation computation times for LST and QST are made significantly smaller by using these closed-form expressions instead of numerical integration.[6]

The ability of tetrahedral elements to model complex shapes, the significant reduction of computation time when replacing numerical integrations by explicit expressions, and the complete polynomial basis of these elements make them extremely well suited to solid modeling applications.

In addition, brick-type elements can be produced by certain combinations of tetrahedral elements. This may be advantageous not only in mesh visualization but also in discretization of the problem domain using combined bricks and tetrahedra.

In the work presented here, the finite element formulation is applied to linear and quadratic strain tetrahedral elements with piezoelectric effects. The element stiffness matrices and equivalent nodal loads are developed in closed form by using a symbolic procedure. Arrangements of tetrahedra to make a hexahedral element are discussed, and the static condensation of resulting interior nodes when the coupled equilibrium equations of piezoelectricity are involved is formulated.

Received Dec. 24, 1993; revision received April 8, 1994; accepted for publication April 8, 1994. Copyright © 1994 by the American Institute of Aeronautics and Astronautics, Inc. All rights reserved.

*Graduate Assistant, Department of Mechanical and Aerospace Engineering.
†Professor, Department of Mechanical and Aerospace Engineering.
‡Associate Professor, Department of Mechanical and Aerospace Engineering. Member AIAA.
§Faculty Associate, Department of Mechanical and Aerospace Engineering. Member AIAA.

Finite Element Formulation

The direct and converse piezoelectric phenomena, which consists of an interaction between the mechanical and electrical behaviors of a material, can be expressed as follows:

$$\{T\} = [C^E]\{S\} - [e]\{E\} \tag{1a}$$

$$\{D\} = [e]^T\{S\} + [\varepsilon^S]\{E\} \tag{1b}$$

Where, using Institute of Radio Engineers (IRE) standards, $\{T\}$ is the stress vector, $[C^E]$ the matrix of elastic coefficients at constant electric field strength, $\{S\}$ the strain vector, $[e]$ the piezoelectric matrix, $\{E\}$ the electric field vector, $\{D\}$ the electric displacement vector, and $[\varepsilon^s]$ the dielectric matrix at constant mechanical strain.

The expressions for the kinetic energy and thermodynamic potential of a piezoelectric media when the effect of damping is neglected are

$$\kappa = \frac{1}{2}\int_V \{\dot{u}\}^T \rho\{\dot{u}\}\,dV \tag{2a}$$

$$\Pi = \frac{1}{2}\int_V (\{S\}^T[C^E]\{S\} - \{S\}^T[e]\{E\} - \{E\}^T[e]^T\{S\} - \{E\}^T[\varepsilon^S]\{E\})\,dV \tag{2b}$$

where $\{\dot{u}\}$ is the time derivative of the displacement vector $\{u\}$, ρ the mass density, and V the volume of the body. The mechanical and electrical work, i.e., W_f and W_q, in the absence of body force, body charge, point forces, and point charges are

$$W_f = \int_{A1} \{u\}^T\{\bar{T}\}\,dA \tag{3a}$$

$$W_q = -\int_{A2} \phi\{\nu\}^T\{D\}\,dA \tag{3b}$$

where $\{\bar{T}\}$ is the surface traction, ϕ is the potential difference, $\{\nu\}$ is the vector of surface direction cosines, and $A1$ and $A2$ are the boundary regions where traction and potential difference are prescribed, respectively. The derivation of electrical work is given in Appendix A.

To obtain a finite element approximation to a general problem defined by Eq. (1), the continuous displacements and electric potential at any point within an element are interpolated from discrete element nodal values using shape function matrices $[N_u]$ and $[N_\phi]$

$$\{u\} = [N_u]\{u_i\} \tag{4a}$$

$$\phi = [N_\phi]\{\phi_i\} \tag{4b}$$

where the respective vectors and matrices are expressed in more detail as follows.

Vector of displacement field

$$\{\boldsymbol{u}\} = [u(x, y, z) \quad v(x, y, z) \quad w(x, y, z)]^T \tag{5a}$$

Electric potential field

$$\phi = \phi(x, y, z) \tag{5b}$$

Matrix of displacement interpolation functions

$$[N_u] = \begin{bmatrix} N_1 & 0 & 0 & N_2 & 0 & 0 \cdots 0 \\ 0 & N_1 & 0 & 0 & N_2 & 0 \cdots 0 \\ 0 & 0 & N_1 & 0 & 0 & N_2 \cdots N_n \end{bmatrix} \tag{5c}$$

Matrix of electric field interpolation functions

$$[N_\phi] = [N_1 \quad N_2 \quad N_3 \cdots N_n] \tag{5d}$$

Element nodal displacements

$$\{u_i\} = [u_1 \quad v_1 \quad w_1 \quad u_2 \cdots w_n]^T \tag{5e}$$

Element nodal electric potentials

$$\{\phi_i\} = \begin{bmatrix} \phi_1 & \phi_2 \cdots \phi_n \end{bmatrix}^T \tag{5f}$$

In the preceding equations, n is the number of nodes employed in defining the finite element. The linear and quadratic interpolation functions for the tetrahedral element (in terms of volume coordinate system) are presented in the next section.

Strains and electric fields are obtained by differentiation.[7,8] Therefore,

$$\{\boldsymbol{S}\} = [\partial]\{\boldsymbol{u}\} = [B_u]\{u_i\} \tag{6}$$

where

$$[B_u] = [\partial][N_u] = \begin{bmatrix} \frac{\partial}{\partial x} & 0 & 0 \\ 0 & \frac{\partial}{\partial y} & 0 \\ 0 & 0 & \frac{\partial}{\partial z} \\ \frac{\partial}{\partial y} & \frac{\partial}{\partial x} & 0 \\ 0 & \frac{\partial}{\partial z} & \frac{\partial}{\partial y} \\ \frac{\partial}{\partial z} & 0 & \frac{\partial}{\partial x} \end{bmatrix} [N_u] \tag{7}$$

and

$$\{\boldsymbol{E}\} = -[\partial]\phi = -[B_\phi]\{\phi_i\} \tag{8}$$

where

$$[B_\phi] = [\partial][N_\phi] = \begin{bmatrix} \frac{\partial}{\partial x} \\ \frac{\partial}{\partial y} \\ \frac{\partial}{\partial z} \end{bmatrix} [N_\phi] \tag{9}$$

Substitution of the expressions for $\{\boldsymbol{u}\}$, $\{\phi\}$, $\{\boldsymbol{S}\}$, and $\{\boldsymbol{E}\}$ into Eqs. (2) yields the kinetic and potential energy expressions for an element e

$$\kappa_e = \tfrac{1}{2}\{\dot{u}_i\}^T[m]\{\dot{u}_i\} \tag{10a}$$

$$\Pi_e = \tfrac{1}{2}\big(\{u_i\}^T[k_{uu}]\{u_i\} + \{u_i\}^T[k_{u\phi}]\{\phi_i\} + \{\phi_i\}^T[k_{\phi u}]\{u_i\} - \{\phi_i\}^T[k_{\phi\phi}]\{\phi_i\}\big) \tag{10b}$$

where the matrices are defined as follows:

Consistent mass matrix

$$[m] = \int_{V_e} [N_u]^T \rho [N_u]\, dV \tag{11}$$

Elastic stiffness matrix

$$[k_{uu}] = \int_{V_e} [B_u]^T [C^E][B_u]\, dV \tag{12}$$

Piezoelectric stiffness matrix

$$[k_{u\phi}] = [k_{\phi u}]^T = \int_{V_e} [B_u]^T [e][B_\phi]\, dV \tag{13}$$

Dielectric stiffness matrix

$$[k_{\phi\phi}] = \int_{V_e} [B_\phi]^T [\varepsilon^S][B_\phi]\, dV \tag{14}$$

Similarly, substituting the expressions for $\{\boldsymbol{u}\}$ and ϕ in Eqs. (3) results in the equivalent generalized loads, that is, the equivalent nodal load vector

$$\{f\}_e = \int_{A_e} [N_u]^T \{\bar{T}\}\, dA \tag{15}$$

and the equivalent nodal charge vector

$$\{q\}_e = -\int_{A_e} [N_\phi]\{\nu\}^T \{\boldsymbol{D}\}\, dA \tag{16}$$

In the preceding, V_e and A_e denote the volume and surface of an element, respectively. Considering $\{u_i\}$ and $\{\phi_i\}$ as the generalized coordinates, and applying the Lagrange's equations gives the equations of motion for each element, i.e.,

$$\frac{d}{dt}\left(\frac{\partial \kappa_e}{\partial\{\dot{u}_i\}}\right) - \frac{\partial \kappa_e}{\partial\{u_i\}} + \frac{\partial \Pi_e}{\partial\{u_i\}} = \{f\}_e \tag{17a}$$

$$\frac{d}{dt}\left(\frac{\partial \kappa_e}{\partial\{\dot{\phi}_i\}}\right) - \frac{\partial \kappa_e}{\partial\{\phi_i\}} + \frac{\partial \Pi_e}{\partial\{\phi_i\}} = \{q\}_e \tag{17b}$$

yield

$$[m]\{\ddot{u}\} + [k_{uu}]\{u_i\} + [k_{u\phi}]\{\phi_i\} = \{f\}_e \tag{18a}$$

$$\{k_{\phi u}\}\{u_i\} - [k_{\phi\phi}]\{\phi_i\} = \{q\}_e \tag{18b}$$

respectively. The element matrices may be assembled to form the representation of the problem in global variables $\{U\}$ and $\{\boldsymbol{\Phi}\}$. Thus,

$$[M]\{\ddot{U}\} + [K_{uu}]\{U\} + [K_{u\phi}]\{\boldsymbol{\Phi}\} = \{F\} \tag{19a}$$

$$[K_{\phi u}]\{U\} - [K_{\phi\phi}]\{\boldsymbol{\Phi}\} = \{Q\} \tag{19b}$$

where

$$[K_{xy}] = \sum^{\text{numel}} [k_{xy}]_e, \qquad [M] = \sum^{\text{numel}} [m]_e, \qquad \{Q\} = \sum^{\text{numel}} \{q\}_e$$

$$\{F\} = \sum^{\text{numel}} \{f\}_e \tag{20}$$

In some applications, such as in sensors, the potential difference vector $\{\boldsymbol{\Phi}\}$ is not of immediate interest, and it may be eliminated by static condensation.[1,2]

Tetrahedral Element Shape Functions

The shape functions for tetrahedral elements are described in terms of a volume coordinate system and are defined as

$$L_i = V_i/V, \qquad i = 1, 2, 3, 4 \tag{21}$$

where V is the volume of the tetrahedron, and V_i is the volume of the subtetrahedron bounded by an interior point and the surface of the tetrahedron opposite node i (Ref. 8). The equations relating the rectangular coordinates of an interior point to the volume coordinates can be expressed as

$$\begin{bmatrix} x \\ y \\ z \\ 1 \end{bmatrix} = \begin{bmatrix} x_1 & x_2 & x_3 & x_4 \\ y_1 & y_2 & y_3 & y_4 \\ z_1 & z_2 & z_3 & z_4 \\ 1 & 1 & 1 & 1 \end{bmatrix} \begin{bmatrix} L_1 \\ L_2 \\ L_3 \\ L_4 \end{bmatrix} \tag{22}$$

and inversely

$$\begin{bmatrix} L_1 \\ L_2 \\ L_3 \\ L_4 \end{bmatrix} = \begin{bmatrix} x_1 & x_2 & x_3 & x_4 \\ y_1 & y_2 & y_3 & y_4 \\ z_1 & z_2 & z_3 & z_4 \\ 1 & 1 & 1 & 1 \end{bmatrix}^{-1} \begin{bmatrix} x \\ y \\ z \\ 1 \end{bmatrix} \tag{23}$$

where x_i, y_i, and z_i are the coordinate locations of the element nodes.

Figure 1a shows the linear strain element LST with 10 nodes and 30 degrees of freedom. The shape functions are given as vertex nodes

$$N_i = (2L_i - 1)L_i, \qquad i = 1, 2, 3, 4 \tag{24a}$$

and midside nodes

$$N_l = 4L_mL_n \qquad l = 5, 6, 7, 8, 9, 10 \tag{24b}$$

where m and n are the vertex nodes of the edge with midside node l.

The quadratic strain tetrahedral element QST assumes 20 nodes, one node at each vertex, two nodes on each of the six edges, and one node at the centroid of each of the four faces (Fig. 1b). The shape functions for the QST element are vertex nodes

$$N_i = (3L_i - 1)(3L_i - 2)(L_i/2), \qquad i = 1, 2, 3, 4 \tag{25a}$$

side nodes

$$N_i = \tfrac{9}{2}L_jL_k(3L_k - 1), \qquad i = 5, 6, \ldots, 16 \tag{25b}$$

and face nodes

$$N_i = 27L_lL_mL_n, \qquad i = 17, 18, 19, 20 \tag{25c}$$

where j and k refer to the vertex nodes closer to the side node, and l, m, and n are the vertex nodes of the face node.[8]

Symbolic Computation

For LST and QST elements all electroelastic stiffness matrices and mass matrices can be evaluated in closed form by means of the equations derived by Eisenberg and Malvern.[9]

$$\int_{\text{volume}} L_1^aL_2^bL_3^c \, dV = \frac{a!b!c!}{(a+b+c+3)!} \times 6 \times \text{volume} \tag{26}$$

Similarly, the equivalent charge and load vectors can be obtained explicitly by using

$$\int_{\text{area}} \xi_1^a\xi_2^b\xi_3^c \, dA = \frac{a!b!c!}{(a+b+c+2)!} \times 2 \times \text{area} \tag{27}$$

where the ξ_i are area coordinates.[7-10]

The symbolic computer system *Mathematica*™ (Ref. 11) was used to generate the closed-form expressions for stiffness matrices and equivalent load and charge vectors. A dramatic savings in element formulation times can be realized as a result of using these explicit expressions in lieu of performing numerical integration.[6]

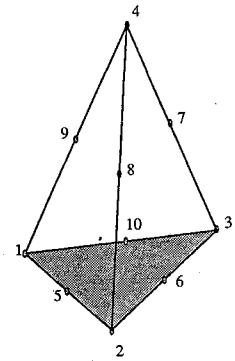

a) LST

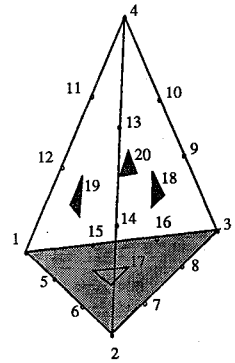

b) QST

Fig. 1 Tetrahedral elements.

Brick-Type Element

Whereas the brick element, because of its simple geometry and ease of visualization, is commonly used in discretization of three-dimensional problem domains, tetrahedral elements may be required to model the regions near the boundary of domains with complex shapes. Brick-type elements can be formed by assembling tetrahedral elements in several ways. Figure 2 illustrates two possible alternatives. Six tetrahedra are combined in alternative Fig. 2a; and the diagonal sides of the opposite faces are parallel, therefore, edge and face node coincidence is insured when all of the adjacent elements are of the same brick-type element. The other arrangement combines five tetrahedra and for compatibility requires the adjacent elements to be alternatively of type Fig. 2b and 2c.

Configuration Fig. 2a with linear strain tetrahedra results in a 27-node brick, whereas, with quadratic strain elements, the brick contains 64 nodes. The interior nodes can be condensed to make a brick having 26 nodes for LST and 56 nodes for QST (Fig. 3).

Assembly and condensation can be done numerically or symbolically. To maximize efficiency, the process of assembling six tetrahedra to form brick element matrices and the condensation operation were performed symbolically using *Mathematica*™ (Ref. 11).

Condensation of Interior Nodes

Degrees of freedom internal to brick-type elements may be eliminated by condensation. The size of the resulting stiffness matrix is reduced. The reduction is more significant in the case of QST brick-type element than for the LST element.

The term representing the effect of inertia in Eq. (19a) is zero for the static loading case. Thus,

$$[K_{uu}]\{U\} + [K_{u\phi}]\{\Phi\} = \{F\} \tag{28a}$$

$$[K_{\phi u}]\{U\} - [K_{\phi\phi}]\{\Phi\} = \{Q\} \tag{28b}$$

The interior node mechanical loadings are zero. Moreover, in a piezoelectric material, charges can exist in the form of bound charges on the boundary surfaces normal to the direction of polarization, which means that the interior node have zero net charges, and the

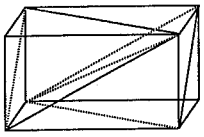

a)

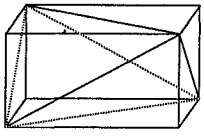

b)

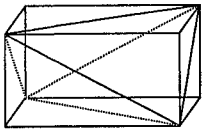

c)

Fig. 2 Various arrangements of tetrahedra to make a brick element: a) six tetrahedra per cube and b) and c) five tetrahedra per cube.

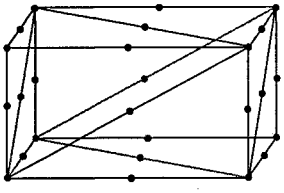

a) LST

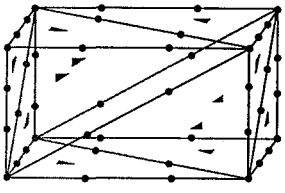

b) QST

Fig. 3 Brick-type elements.

potential difference for these nodes is consequently zero. Therefore, from Eq. (28a)

$$\begin{bmatrix} [K_{uu}^{rr}] & [K_{uu}^{rc}] \\ [K_{uu}^{cr}] & [K_{uu}^{cc}] \end{bmatrix} \begin{pmatrix} \{U^r\} \\ \{U^c\} \end{pmatrix} + \begin{bmatrix} [K_{u\phi}^{rr}] & [K_{u\phi}^{rc}] \\ [K_{u\phi}^{cr}] & [K_{u\phi}^{cc}] \end{bmatrix} \begin{pmatrix} \{\Phi^r\} \\ \{0\} \end{pmatrix} = \begin{pmatrix} \{F^r\} \\ \{0\} \end{pmatrix} \tag{29}$$

where $\{U^r\}$ and $\{\Phi^r\}$ are DOF to be retained, and $\{U^c\}$ are internal DOF to be eliminated by condensation. Eliminating $\{U^c\}$ from Eq. (29) yields

$$\left([K_{uu}^{rr}] - [K_{uu}^{rc}][K_{uu}^{cc}]^{-1}[K_{uu}^{cr}]\right)\{U^r\} + \left([K_{u\phi}^{rr}] - [K_{uu}^{rc}] \times [K_{uu}^{cc}]^{-1}[K_{u\phi}^{cr}]\right)\{\Phi^r\} = \{F^r\} \tag{30}$$

Similarly from Eq. (28b)

$$\begin{bmatrix} [K_{\phi u}^{rr}] & [K_{\phi u}^{rc}] \\ [K_{\phi u}^{cr}] & [K_{\phi u}^{cc}] \end{bmatrix} \begin{pmatrix} \{U^r\} \\ \{U^c\} \end{pmatrix} - \begin{bmatrix} [K_{\phi\phi}^{rr}] & [K_{\phi\phi}^{rc}] \\ [K_{\phi\phi}^{cr}] & [K_{\phi\phi}^{cc}] \end{bmatrix} \begin{pmatrix} \{\Phi^r\} \\ \{0\} \end{pmatrix} = \begin{pmatrix} \{Q^r\} \\ \{0\} \end{pmatrix} \tag{31}$$

Evaluating $\{U^c\}$ from Eq. (29) and substituting into Eq. (31) gives

$$\{U^c\} = -[K_{uu}^{cc}]^{-1}\left([K_{u\phi}^{cr}]\{\Phi^r\} + [K_{uu}^{cr}]\{U^r\}\right) \tag{32}$$

$$\left([K_{\phi u}^{rr}] - [K_{\phi u}^{rc}][K_{uu}^{cc}]^{-1}[K_{uu}^{cr}]\right)\{U^r\} - \left([K_{\phi\phi}^{rr}] + [K_{\phi u}^{rc}][K_{uu}^{cc}]^{-1}[K_{u\phi}^{cr}]\right)\{\Phi^r\} = \{Q^r\} \tag{33}$$

Thus, the condensed electroelastic stiffness matrices from Eqs. (30) and (33) become the following.

Elastic stiffness matrix:

$$[k_{uu}^{\text{brick}}] = [K_{uu}^{rr}] - [K_{uu}^{rc}][K_{uu}^{cc}]^{-1}[K_{uu}^{cr}] \tag{34}$$

Piezoelectric stiffness matrix:

$$[k_{u\phi}^{\text{brick}}] = [k_{\phi u}^{\text{brick}}]^T = [K_{u\phi}^{rr}] - [K_{uu}^{rc}][K_{uu}^{cc}]^{-1}[K_{u\phi}^{cr}] \tag{35}$$

Dielectric stiffness matrix:

$$[k_{\phi\phi}^{\text{brick}}] = [K_{\phi\phi}^{rr}] + [K_{\phi u}^{rc}][K_{uu}^{cc}]^{-1}[K_{u\phi}^{cr}] \tag{36}$$

Numerical Examples

To demonstrate the validity of the closed-form expressions for LST and QST elements and to verify the condensed electroelastic stiffness matrices for the brick-type element, two numerical examples are considered. In the first example the actuator mode of a bimorph piezoelectric beam which consists of two piezoceramic layers with the same polarity is examined. The second example studies the sensor mode of a piezoceramic cube subjected to uniform axial pressure. In both cases the material is piezoceramic PZT-4 whose properties are summarized in Table 1 (Ref. 12).

Actuator Example

Two piezoceramic beams with the same polarity are bonded together and fixed at one end to form a cantilever beam, Fig. 4. Applying a dc voltage in parallel connection across the thickness results in the axial contraction of one layer and the axial extension of the other one. The outcome of this electrical excitation is a static transverse deflection.

Each layer of the cantilever beam is modeled with 25 elements; Fig. 5 illustrates the finite element model and its deformed shape. The deflection of the beam at several points along the neutral plane was obtained for an applied electric potential of 100 V. Figure 6 shows a comparison of the calculated results with the theoretical solution. The theoretical solution is given by $w(x) =$

Table 1 Material properties for PZT-4

Elastic, N/m^2	Piezoelectric, C/m^2	Dielectric, N/V^2
C_{11}^E 13.9 $E10$	e_{13} −5.2	ε_{11} 6.45 E-9
C_{12}^E 6.78 $E10$	e_{23} −5.2	ε_{22} 6.45 E-9
C_{13}^E 7.43 $E10$	e_{33} 15.1	ε_{33} 5.62 E-9
C_{33}^E 11.5 $E10$	e_{42} 12.7	
C_{44}^E 2.56 $E10$	e_{15} 12.7	
C_{66}^E 3.56 $E10$		

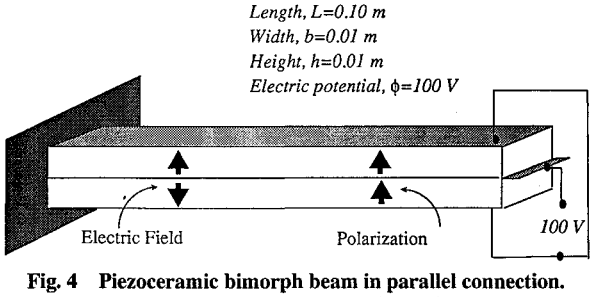

Fig. 4 Piezoceramic bimorph beam in parallel connection.

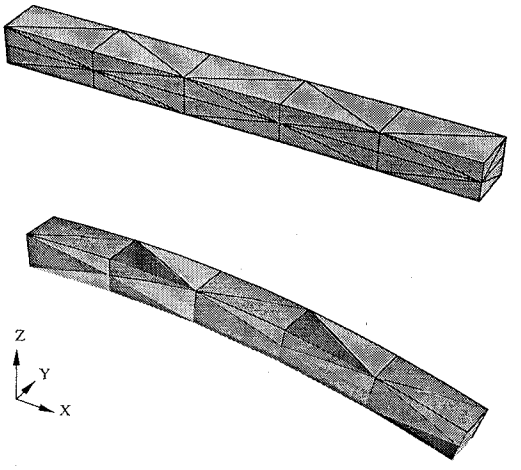

Fig. 5 Finite element model and deformed shape (exaggerated).

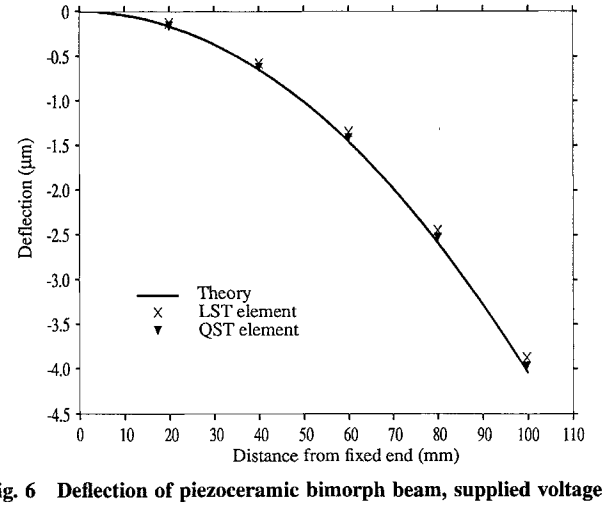

Fig. 6 Deflection of piezoceramic bimorph beam, supplied voltage = 100 V.

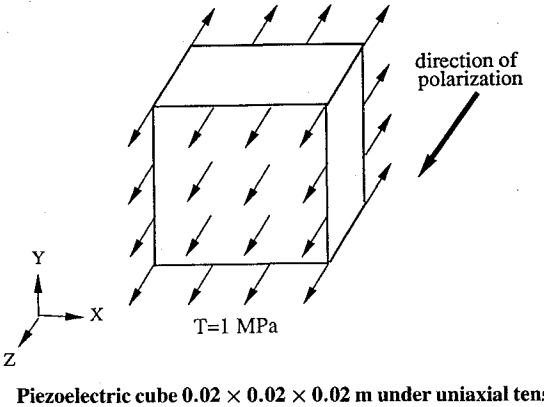

Fig. 7 Piezoelectric cube 0.02 × 0.02 × 0.02 m under uniaxial tension.

$[-3(d_{31}\phi/h^2)x^2]$ where d_{31} is the piezoelectric constant obtained from $[d] = [C^E]^{-1}[e]$; h is the total thickness of the beam; ϕ is the electric potential, that is, voltage; and x is the distance from the fixed end (see Appendix B for a derivation of the theoretical result).

Sensor Example

In this example the elementary problem of a piezoelectric cube subjected to uniform axial pressure is examined. The geometry and applied load are shown in Fig. 7. Because of the symmetry of load and geometry, only one-eighth of the cube need be considered, Fig. 8. The exact absolute value of the charge density $\bar{Q}$, which is developed on the surfaces normal to the direction of polarization,

Table 2 Nodal charges for LST brick-type element

Node	1	2	3	4	5	6	7	8	9
Charge 10^{-8}C	0	0.509	0	0.509	1.019	0.509	0	0.509	0

Table 3 Nodal charges for QST brick-type element

Node	Charge 10^{-8}C	Node	Charge 10^{-8}C
1	1.019	9	1.146
2	1.146	10	6.879
3	1.146	11	2.293
4	0.509	12	1.146
5	1.146	13	0.509
6	2.293	14	1.146
7	6.879	15	1.146
8	1.146	16	1.019

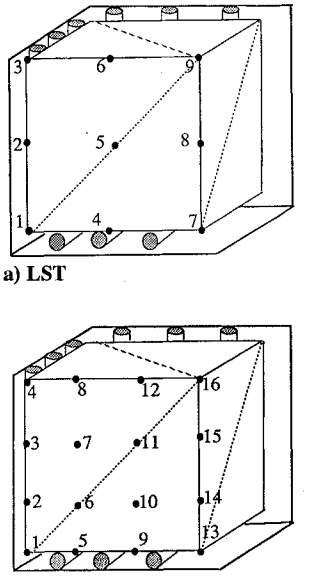

Fig. 8 Finite element models.

is given by $\bar{Q} = |Td_{33}|$ where d_{33} is the piezoelectric constant. Both linear strain and quadratic strain brick-type elements are used to model the cube. The nodal charges developed due to an external pressure of 1 Mpa are listed in Tables 2 and 3. The node numbering for these nodal charges is specified in Fig. 8. The charge density for both models are calculated as $30 \times 10^{-5}(C/m^2)$ which is in agreement with the theoretical values. [It should be noted that the LST element corner nodes do not carry any charges, and the nonzero values always appears at the midside nodes. This is solely due to the properties of the LST shape functions that were used in Eqs. (24). Different results would be expected if different shape functions were used.]

Conclusion

The finite element formulation has been implemented for linear and quadratic strain tetrahedral elements with piezoelectric effects. The closed-form expressions for electroelastic stiffness matrices and equivalent nodal loads and charges are developed. Significant time savings which can be achieved when explicit expressions are used as compared with numerical integration was discussed.

A brick-type element which can simplify the mesh visualization and problem domain discretization when using combined tetrahedra and bricks was presented, and the static condensation of the interior nodes for the brick-type element was formulated. Numerical examples which demonstrate the validity of the development have been presented.

Appendix A: Derivation of the Electrical Work

The electrical work in terms of electric displacement $\{D\}$ and electric field $\{E\}$ is

$$W_q = \int_V \{D\}^T \{E\}\, dV \tag{A1}$$

where V is the volume. The electric field $\{E\}$ in terms of the potential difference ϕ can be expressed as

$$\{E\} = -\{\nabla\}\phi \tag{A2}$$

where

$$\{\nabla\} = \left[\frac{\partial}{\partial x}\ \frac{\partial}{\partial y}\ \frac{\partial}{\partial z}\right]^T$$

is the vector differential operator. Substituting Eq. (A2) into Eq. (A1) and using the following vector identity

$$\{\nabla\}^T(\phi\{D\}) = \phi(\{\nabla\}^T\{D\}) + \{D\}^T(\{\nabla\}\phi) \tag{A3}$$

gives

$$\begin{aligned} W_q &= -\int_V \{D\}^T(\{\nabla\}\phi)\, dV \\ &= -\int_V \{\nabla\}^T(\phi\{D\})\, dV + \int_V \phi(\{\nabla\}^T\{D\})\, dV \end{aligned} \tag{A4}$$

From Maxwell's equation it can be written

$$\{\nabla\}^T\{D\} = \rho_f \tag{A5}$$

where ρ_f is the free-charge density.[12] For piezoelectric materials which are considered to be polarizable but not magnetizable $\rho_f = 0$, therefore, the second term in Eq. (A3) becomes zero. Thus,

$$W_q = -\int_V \{\nabla\}^T(\phi\{D\})\, dV \tag{A6}$$

Applying the divergence theorem to Eq. (A6) results in

$$W_q = -\int_A \phi\{\nu\}^T\{D\}\, dA \tag{A7}$$

where $\{\nu\}$ is the vector of surface direction cosines and A is the area.

Appendix B: Derivation of the Transverse Deflection for Piezoelectric Bimorph Beam

The derivation of deflection is based on the assumptions involved in the classical (Euler-Bernoulli) beam theory. According to this theory, which is applicable to the beams with $h/L \ll 1$ and $b/h \ll 1$ (see Fig. B1), a plane initially normal to the midsurface remains plane and normal and without strain in the thickness direction. Additionally, all of the action, loads, and responses are in the x-z plane, and there are no stresses, strains, displacements, or loads in the y direction.[13] These assumptions, accordingly, require that

$$S_z = S_y = S_{xz} = S_{yz} = v_0 = 0 \tag{B1}$$

$$u(x) = u_0 - z\frac{\partial w}{\partial x} \tag{B2}$$

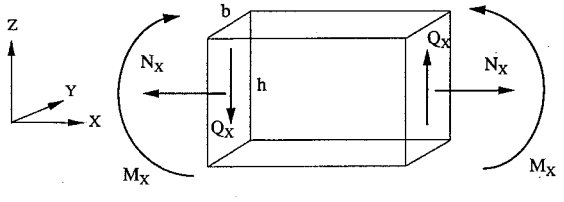

Fig. B1 Stress resultants.

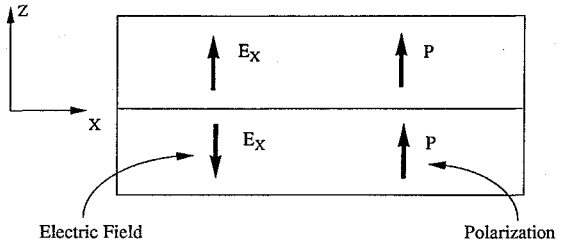

Fig. B2 Electric field and polarization in parallel connection.

where u_0 and v_0 are the in-plane middle surface displacements ($z = 0$), and w is the lateral deflection. Figure B1 shows the stress quantities for the beam when subjected to the lateral and in-plane loads.

The constitutive equation representing the direct piezoelectric effect is[12]

$$\{S\} = [S^E]\{T\} + [d]\{E\} \tag{B3}$$

where $[S^E]$ is the compliance matrix at constant electric field strength. For transversely isotropic piezoceramics, this equation can be expressed as

$$\begin{bmatrix} S_x \\ S_y \\ S_z \\ S_{xy} \\ S_{xz} \\ S_{yz} \end{bmatrix} = \begin{bmatrix} S_{11}^E & S_{12}^E & S_{13}^E & 0 & 0 & 0 \\ S_{12}^E & S_{11}^E & S_{13}^E & 0 & 0 & 0 \\ S_{13}^E & S_{13}^E & S_{33}^E & 0 & 0 & 0 \\ 0 & 0 & 0 & S_{44}^E & 0 & 0 \\ 0 & 0 & 0 & 0 & S_{44}^E & 0 \\ 0 & 0 & 0 & 0 & 0 & \dfrac{S_{11}^E - S_{12}^E}{2} \end{bmatrix} \begin{bmatrix} T_x \\ T_y \\ T_z \\ T_{xy} \\ T_{xz} \\ T_{yz} \end{bmatrix}$$

$$+ \begin{bmatrix} 0 & 0 & d_{31} \\ 0 & 0 & d_{31} \\ 0 & 0 & d_{33} \\ 0 & d_{15} & 0 \\ d_{15} & 0 & 0 \\ 0 & 0 & 0 \end{bmatrix} \begin{bmatrix} E_x \\ E_y \\ E_z \end{bmatrix} \tag{B4}$$

Introducing the assumptions for classical beam theory into the preceding relations and considering only the first equation results in

$$\frac{1}{S_{11}^E}\left(\frac{\partial u_0}{\partial x} - z\frac{\partial^2 w}{\partial x^2}\right) = T_x + \frac{d_{31}}{S_{11}^E}E_z \tag{B5}$$

Multiplying Eq. (B4) by $z\ dz$ and integrating across the thickness yields

$$\left(-\frac{h^3}{12S_{11}^E}\right)\frac{\partial^2 w}{\partial x^2} = M_x + M_x^* \tag{B6}$$

where

$$M_x^* = \int_{(-h/2)}^{h/2} \frac{d_{31}}{S_{11}^E} E_z z\, dz, \qquad M_x = \int_{(-h/2)}^{h/2} T_x z\, dz \tag{B7}$$

For a piezoelectric bimorph beam, when no mechanical loads are applied, $M_x = 0$, therefore,

$$\left(-\frac{h^3}{12S_{11}^E}\right)\frac{\partial^2 w}{\partial x^2} = M_x^* \tag{B8}$$

Moreover, for the same beam in electrical parallel connection when the thickness for each layer is constant, Fig. B2, the electric field is for the upper beam: $E_z = 2(\phi/h)$ and for the lower beam: $E_z = -2(\phi/h)$. Substituting E_z in Eq. (B6), gives the expression for the bending moment due to piezoelectric actuation, i.e.,

$$\begin{aligned} M_x^* &= \int_{-(h/2)}^{h/2} \frac{d_{31}}{S_{11}^E} E_z z\, dz = -\int_{-(h/2)}^{0} 2\frac{d_{31}}{S_{11}^E h}\phi z\, dz \\ &+ \int_0^{h/2} 2\frac{d_{31}}{S_{11}^E h}\phi z\, dz = \frac{d_{31}\phi h}{2S_{11}^E} \end{aligned} \tag{B9}$$

Thus, the governing differential equation of piezoelectric bimorph beam in parallel connection, on substitution of Eq. (B8) into Eq. (B7), is determined to be

$$\frac{\partial^2 w}{\partial x^2} = -6\frac{d_{31}\phi}{h^2} \tag{B10}$$

Solving Eq. (B10) and applying the boundary conditions for a cantilever beam, i.e., $w = \partial w/\partial x = 0$ at $x = 0$, gives the following expression for the transverse deflection of a piezoelectric bimorph beam:

$$w(x) = -3\frac{d_{31}\phi}{h^2}x^2 \tag{B11}$$

Acknowledgment

The authors wish to thank the reviewers for their helpful comments.

References

[1]Allik, H., and Hughes, T. J. R., "Finite Element Method for Piezoelectric Vibration," *International Journal for Numerical Methods in Engineering*, Vol. 2, April 1970, pp. 151–157.

[2]Tzou, H. S., and Tseng, C. I., "Distributed Piezoelectric Sensor/Actuator Design for Dynamic Measurement/Control of Distributed Parameter System: A Piezoelectric Finite Element Approach," *Journal of Sound and Vibration*, Vol. 138, Jan. 1990, pp. 17–34.

[3]Ha, S. K., Keilers, C., and Chang, F. K., "Finite Element Analysis of Composite Structures Containing Distributed Piezoelectric Sensors and Actuators," *AIAA Journal*, Vol. 30, No. 3, 1992, pp. 772–780.

[4]Wong, K. A., "Symbolic Computing: Numerical and Computer Methods," *Structural Mechanics*, edited by S. J., Fenves et al., Academic Press, New York, 1973.

[5]Lawrence, K. L., Nambiar, R. V., and Bergman, B., "Closed Form Stiffness Matrices and Error Estimators for Plane Hierarchic Triangular Finite Elements," *International Journal for Numerical Methods in Engineering*, Vol. 31, April 1991, pp. 879–894.

[6]Shiakolas, P. S., Nambiar, R. V., Lawrence, K. L., and Rogers, W. A., "Closed Form Stiffness Matrices for the Linear Strain and Quadratic Strain Tetrahedron Finite Elements," *Computers and Structures*, Vol. 45, No. 2, 1992, pp. 237–242.

[7]Cook, R. D., Malkus, D. S., and Plesha, M. E., *Concepts and Applications of Finite Element Analysis*, 3rd ed., John Wiley and Sons, New York, 1989.

[8]Zienkiewicz, O. C., and Taylor, R. L., *The Finite Element Method, Basic Formulation and Linear Problems*, Vol. 1, McGraw-Hill, London, 1989.

[9]Eisenberg, M. A., and Malvern, L. E., "On Finite Element Integration in Natural Coordinates," *International Journal for Numerical Methods in Engineering*, Vol. 7, July 1973, pp. 574, 575.

[10]Stricklin, J. A., "Integration of Area Coordinates in Matrix Structural Analysis," *AIAA Journal*, Vol. 6, No. 10, 1968, p. 2023.

[11]Wolfram, S., *Mathematica, A System for Doing Mathematics by Computer*, Addison-Wesley, Redwood City, CA, 1992.

[12]Parton, V. Z., and Kudryavtsev, B. A., *Electromagnetoelasticity Piezoelectrics and Electrically Conductive Solids*, Gordon and Breach Science, New York, 1988.

[13]Vinson, J. R., *The Behavior of Thin Walled Structures*, Kluwer Academic, The Netherlands, 1989.